J. Eur. Opt. Society-Rapid Publ. 2023, **19**, 2

https://doi.org/10.1051/jeos/2022015
Available online at: https://jeos.edpsciences.org

Journal of the European Optical Society-Rapid Publications

EOSAM 2022
Guest editors: Patricia Segonds, Gilles Pauliat and Emiliano Descrovi

SHORT COMMUNICATION OPEN ACCESS

Wavelength-switchable L-band fiber laser assisted by random reflectors

R.A. Perez-Herrera[1,2,*], P. Roldan-Varona[3,4,5], A. Sanchez-Gonzalez[1,2], L. Rodriguez-Cobo[4], J.M. Lopez-Higuera[3,4,5], and M. Lopez-Amo[1,2]

[1] Department of Electrical, Electronic and Communication Engineering, Public University of Navarra, 31006 Pamplona, Spain
[2] Institute of Smart Cities (ISC), Public University of Navarra, 31006 Pamplona, Spain
[3] Photonics Engineering Group, University of Cantabria, 39005 Santander, Spain
[4] CIBER-bbn, Instituto de Salud Carlos III, 28029 Madrid, Spain
[5] Instituto de Investigacion Sanitaria Valdecilla (IDIVAL), 39005 Cantabria, Spain

Received 18 October 2022 / Accepted 5 December 2022

Abstract. A wavelength-switchable L-band erbium-doped fiber laser (EDFL) assisted by an artificially controlled backscattering (ACB) fiber reflector is here presented. This random reflector was inscribed by femtosecond (fs) laser direct writing on the axial axis of a multimode fiber with 50 μm core and 125 μm cladding with a length of 17 mm. This microstructure was placed inside a surgical syringe to be positioned in the center of a high-precision rotation mount to accurately control its angle of rotation. Only by rotating this mount, three different output spectra were obtained: a single wavelength lasing centered at 1574.75 nm, a dual wavelength lasing centered at 1574.75 nm and 1575.75 nm, and a single wavelength lasing centered at 1575.5 nm. All of them showed an optical signal-to-noise ratio (OSNR) of around 60 dB when pumped at 300 mW.

Keywords: Fiber laser, L-band, Random reflector, Wavelength-switchable.

1 Introduction

Femtosecond (fs) laser writing has become an effective way to process any type of transparent optical material, such as silica optical fibers [1]. This technology enables the microfabrication of numerous fiber structures with excellent properties for a wide range of practical applications [2]. In particular, the development of fiber-optic microstructures based on refractive index (RI) modification under fs-laser irradiation has resulted in different implementations in the field of optical fiber sensors: surrounding refractive index sensors [3], strain sensors [4], curvature sensors [5], or multiparameter sensors [6], among others. These artificially controlled backscattering (ACB) fiber reflectors have been shown to have similar temperature sensitivity to traditional FBGs. However, the strain sensitivity can be improved by more than an order of magnitude when comparing these quasi-randomly distributed reflective microstructures with FBG-based sensors [7].

In addition to the above, these fiber-optic microstructures also have interesting applications in areas such as fiber-optic lasers [8], fiber Bragg gratings (FBGs) [9], long period fiber gratings (LPGs) [10], tilted fiber Bragg gratings [11], interferometers [12–14], couplers [15] or birefringence adjustable elements [1, 16]. In further, changes in the birefringence of a fiber can be caused by its twist [17]. Investigation of twist induced birefringence has been a topic of investigation back to the late 1970s, early 1980s [18–20] and continued up to recent years [21, 22]. One of the most important parameters in these studies is the evolution of the polarization dependent loss (PDL) response of the fiber-based reflector with respect to the applied twist [23]. As presented in [23], the PDL response of a fiber grating structure has higher twist sensitivity than that of the reflected or transmitted amplitude spectrum. Moreover, PDL shows two distinct lobes whose changes with the increase/decrease of twist angle are significant (both in counter clock and clockwise twist), providing meaningful information for the twist effects.

In this work, an artificially controlled backscattering (ACB) fiber reflector inscribed by fs laser direct-write technique is used into an L-band erbium doped fiber laser (EDFL). This random reflector was inscribed on the axial axis of a 50/125 multimode fiber (MMF), with a length of 17 mm, and located into a high-precision rotation mount to control its angle of twist rotation. Only by rotating in

* Corresponding author: rosa.perez@unavarra.es

a range of 8° the MMF sample where the RFG was inscribed, this wavelength-switchable EDFL can be switched among three different lasing spectra: a single wavelength lasing centered at 1574.75 nm, a dual wavelength lasing centered at 1574.75 nm and 1575.75 nm, or a single wavelength lasing centered at 1575.5 nm. An OSNR of 60 dB and 58 dB were measured for single and dual-wavelength operation respectively, when pumped at 300 mW.

2 Fabrication and characterization process

An ACB multimode fiber reflector was inscribed by using ultrafast laser writing, performed by a Cazadero fiber laser (Calmar Laser) that delivers 370 fs laser pulses at a central wavelength of 1030 nm. It is worth noting that, as presented in [24], the light absorbed non-linearly by the fiber has a wavelength of 515 nm, due to the second harmonic generation (SHG) introduced in the setup. The laser pulses were tightly focused into the Ø50 μm core of the MMF using a 0.42 NA, 50× objective lens from Mitutoyo. A pulse energy of 0.75 μJ and a pulse repetition rate (PRR) of 150 Hz were used, and the MMF sample was translated through the laser focus using a motorized nano-resolution *XYZ* stage from Aerotech. This ACB MMF reflector had a random period between $\Lambda_{\min} = 1.61085$ μm and $\Lambda_{\max} = 1.64230$ μm, with a length of 17 mm. It was also written on the axial axis of the MMF. Although this is a random fiber grating (MMF-RFG) [25], the almost total periodicity of the optical structure gives rise to Bragg resonances which, in the third order ($m = 3$) and with an effective refractive index (n_{eff}) of around 1.4528, present reflections in the following spectral band:

$$\lambda_B = \frac{2}{m} n_{eff} \Lambda \approx 1575.4\,\text{nm}. \quad (1)$$

Before placing this MMF-RFG inside the surgical syringe to be positioned in the center of a high-precision rotation mount, its backscattered optical power was characterized with an optical frequency domain reflectometer (OFDR). This ultra-high spatial resolution optical backscattered reflectometer (OBR 4600, from LUNA) is commonly used not only for optical sensing of strain and temperature variations but to test fiber optic components, optical fibers and optical fiber sensors [26]. Free termination of this fiber-based reflector was immersed into index-matching oil to avoid undesired reflections.

Figure 1a presents the backscattered optical power as a function of fiber length for the inscribed MMF-RFG. As this figure shows, the MMF sample was located about 1.88 m from the connector of the OBR and it showed an amplitude between 40 and 50 dB above the noise level. Figure 1b illustrates the reflection spectrum of the MMF-RFG reflector. This spectrum shows a non-flat response, with a maximum value of around −10 dB at around 1575.5 nm, so it is expected that the emission wavelengths of the generated lasers will be mainly determined by the shape of this spectrum.

3 Experimental setup

Figure 2 illustrates a schematic diagram of the L-band linear-cavity fiber laser experimental setup. As this figure shows, the 976-nm pump power (Fig. 2a) was injected into the linear-cavity EDFL by means of a 980/1550 nm wavelength division multiplexer (WDM) (Fig. 2b). The gain medium was 5 m of highly erbium-doped fiber (EDF) I25 (980/125, Fibercore Inc.) (Fig. 2c), suitable for C-band amplifiers with a core composition optimized for EDF amplifiers (EDFAs) in dense-WDM (DWDM) networks and a peak core absorption ranges from 7.7 to 9.4 dB/m at 1531 nm [27]. This EDF was connected to the common port of the WDM and followed by a 3-ports optical circulator (Fig. 2d) in which ports 3 and 1 were connected to conform a fiber loop mirror (FLM), as in [27]. After passing through the highly EDF section again, the reflected signal from the FLM arrived to the 1550 nm-port of the WDM up to the optical coupler (Fig. 2e). Then, the signal is divided into two branches where 90% of the signal reached the MMF-RFG-based reflector and the other 10% was visualized with an optical spectrum analyzer (OSA) (Fig. 2f) with a resolution of 30 pm and a sensitivity of −75 dBm. The section of fiber where the MMF-RFG was inscribed was placed inside a surgical syringe so that it could be positioned in the center of the high-precision rotation mount (Fig. 2g) to accurately control its angle of rotation. A photograph of the RFG reflector inscribed by femtosecond laser writing is shown in Figure 2h. As in previous studies, free end of the ACB fiber-based reflector was immersed in refractive index-matching gel to avoid undesired reflections. All the experimental measurements were carried out at room temperature, and no vibration isolation or temperature compensation techniques were employed.

4 Results and discussion

Figure 3a depicts the relation between the output power levels as a function of the injected 976 nm pump power when single-wavelength operation centered at 1574.75 nm (blue line) or centered at 1575.75 nm (red line) were obtained. Similarly, Figure 3b presents the same relation between pump power levels versus output power but when simultaneous dual-wavelength emission centered at 1574.75 nm (blue line) and centered at 1575.75 nm (red line) was reached. As Figure 3b illustrates, the power level of both lasers increases evenly as pumping power increases. Moreover, a pump power threshold of around 50 mW with and an optical efficiency of 0.26% were measured when the EDFL was tuned to obtain a single-longitudinal laser emission. This pump power threshold value increased 5 mW when dual-wavelength emission is obtained, while maintaining the same total optical efficiency than the previous case, as shown in (Fig. 3b).

Figure 4 shows the output spectra of the linear cavity EDF pumped at 300 mW when (a) single-wavelength laser emission centered at 1574.75 nm, (b) dual-wavelength laser emission centered at 1574.75 nm and 1575.53 nm, or (c) single-wavelength laser emission line at 1575.53 nm

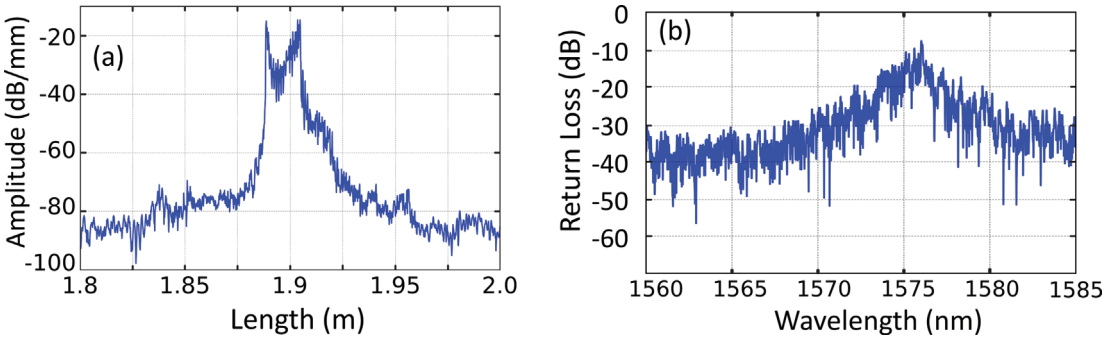

Figure 1. Backscattered optical power as a function of fiber length for the MMF-RFG, located about 1.88 m from the connector of the OBR (a) and reflected power as a function of the wavelength for the MMF-RFG reflector (b).

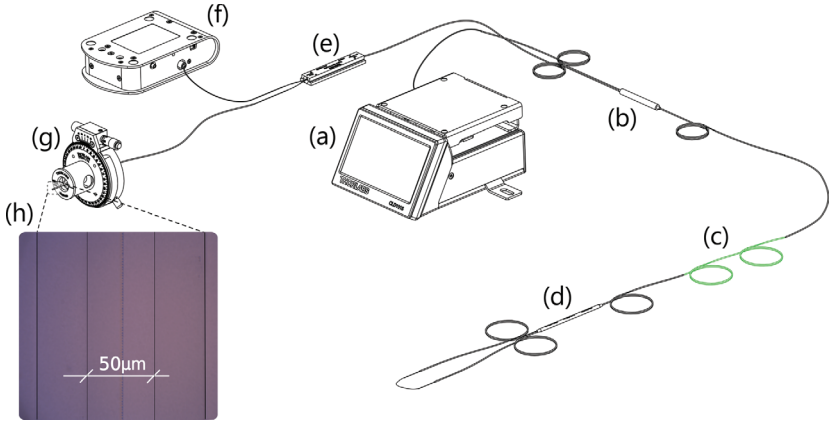

Figure 2. Schematic diagram of the experimental L-band linear-cavity fiber laser setup; (a) pump laser; (b) wavelength-division multiplexer; (c) erbium-doped fiber; (d) fiber optic circulator; (e) optical coupler; (f) optical spectrum analyzer; (g) high-precision rotation mount where the MMF-RFG was rotated; (h) photograph of the inscribed MMF-RFG located into a syringe.

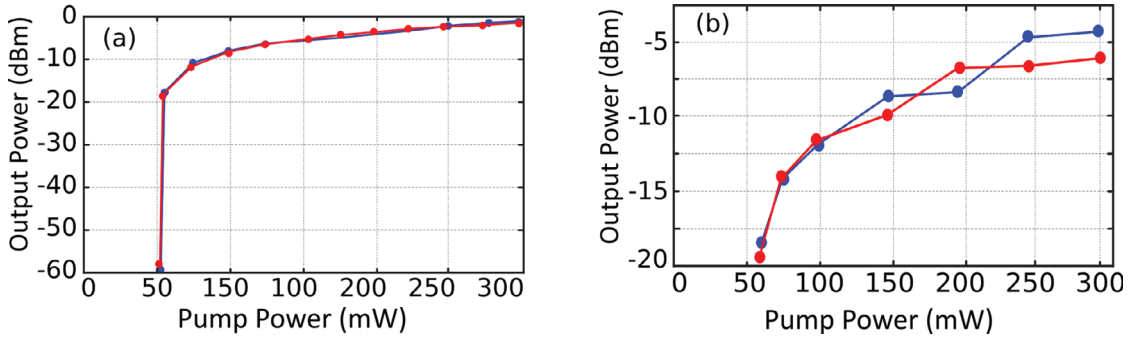

Figure 3. Relationship between the output-power levels versus 976-nm pump power when (a) single-wavelength operation centered at 1574.75 nm (blue line) or at 1575.75 nm (red line) and (b) dual-wavelength operation were obtained.

were obtained. By rotating the high-precision rotation mount where the multimode fiber-based reflector was located into a syringe, these three configurations can be easily reached. Output power levels of −1.02 dBm (Fig. 4a) and −1.85 dBm (Fig. 4c) were measured when single-wavelength laser emission was attained, both presenting an OSNR of 60 dB. On the other hand, when dual-wavelength laser emission was achieved, an output power level around −5 dBm and an OSNR of 58 dB was measured (Fig. 4b). As expected, by increasing the number of lasing wavelengths the output power values of the lasing emission lines decrease [28].

Figure 4d illustrates the frequency spectrum corresponding to the frequency domain conversion, when a photodetector in combination with an ESA was used to evaluate the longitudinal laser mode behavior. As in [29], heterodyne detection was carried out by using a 3-dB optical coupler for mixing the signal from a tunable laser source

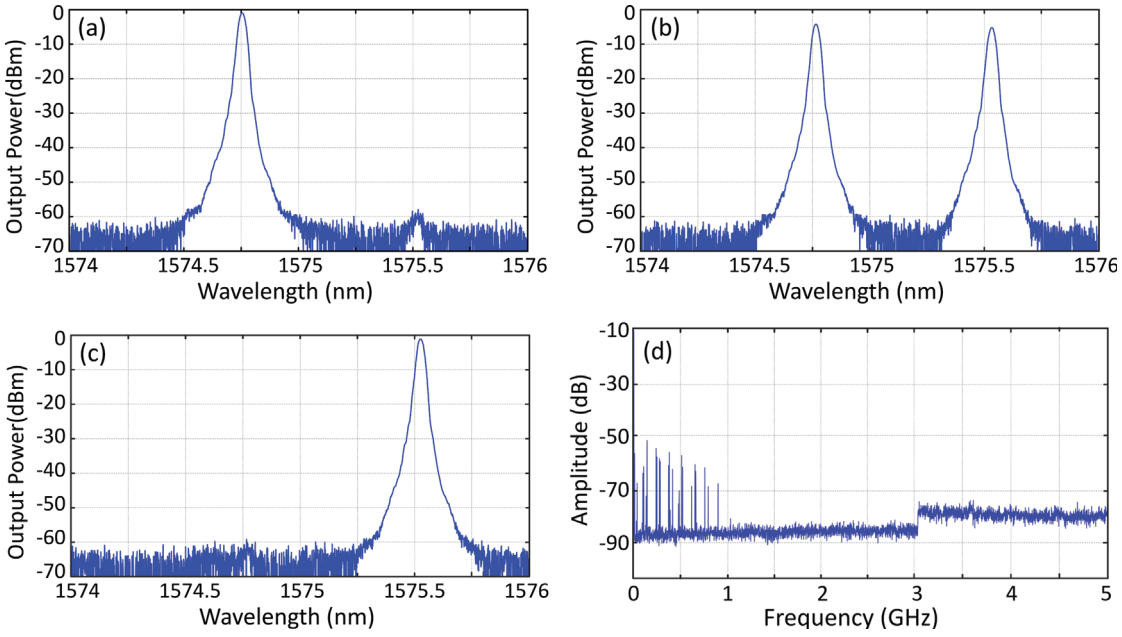

Figure 4. Output spectra of the linear-cavity fiber laser with a MMF-RFG reflector pumped by a 976-nm laser, when (a) a single wavelength lasing centered at 1574.75 nm, (b) a dual wavelength lasing centered at 1574.75 nm and 1575.75 nm, and (c) a single wavelength lasing centered at 1575.5 nm are obtained. (d) Electric beat with a tunable laser source (TLS) of the single-wavelength lasing emission when pumped at 300 mW.

(TLS) whose full width at half-maximum (FWHM) linewidth was 100 kHz, with the reflected signal from the MMF-RFG-based reflector. This measured frequency spectrum clearly shows the appearance of multiple longitudinal mode beating, demonstrating its multimode operation.

Such multimode lasers are usually more unstable that single mode ones in their output power levels. However, in this case, an output power level variation of 0.28 dB, with a confidence level (CL) of 95% was measured at room temperature. Measured data was stored each 10 s for 1 h, when single wavelength lasing pumped at 300 mW with a FWHM of 28.05 pm was obtained. The central emission wavelength of this laser showed a variation of 23 pm during the same period but with a CL of 100%.

5 Conclusions

In this work, a new wavelength-switchable L-band erbium-doped fiber laser is proposed and experimentally characterized. The laser is assisted by an artificially controlled backscattering fiber reflector, inscribed by femtosecond laser writing. This reflector is a random fiber grating that was written on the axial axis of a 50/125 multimode fiber with a length of 17 mm. This quasi-distributed fiber reflector was placed inside a surgical syringe to be positioned in the center of a high-precision rotation mount to precisely control its angle of rotation. Only by rotating this mount, three different output spectra were obtained: a single wavelength lasing centered at 1574.75 nm, a dual wavelength lasing centered at 1574.75 nm and 1575.75 nm, and a single wavelength lasing centered at 1575.5 nm. All of them showed an optical signal-to-noise ratio of 60 dB when pumped at 300 mW.

Acknowledgments. This work was financed by the program "José Castillejo para estancias de movilidad en el extranjero de jóvenes doctores", funded by the Ministerio de Universidades of Spain (reference CAS21/00351); the Spanish AEI projects PID2019-107270RB, funded by MCIN/AEI/10.13039/501100011033 and FEDER "A way to make Europe", and projects PDC2021-121172 and TED2021-130378B funded by MCIN/ AEI/ 10.13039/501100011033 and European Union "Next generation EU"/PTR. Finally, the work was also founded by the Ministerio de Educación, Cultura y Deporte of Spain (PhD grant FPU2018/02797).

References

1 Zhao J., Zhao Y., Peng Y., Lv R.-Q., Zhao Q. (2022) Review of femtosecond laser direct writing fiber-optic structures based on refractive index modification and their applications, *Opt. Laser Technol.* **146**, 107473.
2 Chen M., He T., Zhao Y. (2022) Review of femtosecond laser machining technologies for optical fiber microstructures fabrication, *Opt. Laser Technol.* **147**, 107628.
3 Chen P.C., Shu X.W., Cao H.Y., Sugden K. (2017) Ultra-sensitive refractive index sensor based on extremely simple femtosecond-laser-induced structure, *Opt. Lett.* **42**, 6, 1157–1160.
4 Deng J., Wang D.N. (2019) Ultra-sensitive strain sensor based on femtosecond laser inscribed in-fiber reflection mirrors and Vernier effect, *J. Light. Technol.* **37**, 19, 4935–4939.

5 Yakushin S.S., Wolf A.A., Dostovalov A.V., Skvortsov M.I., Wabnitz S., Babin S.A. (2018) A study of bending effect on the femtosecond-pulse inscribed fiber Bragg gratings in a dual-core fiber, *Opt. Fiber Technol.* **43**, 101–105.

6 Leal-Junior A.G., Theodosiou A., Díaz C.R., Marques C., José Pontes M., Kalli K., Frizera A. (2019) Simultaneous measurement of axial strain, bending and torsion with a single fiber Bragg grating in CYTOP fiber, *J. Light. Technol.* **37**, 3, 971–980.

7 Perez-Herrera R.A., Bravo M., Roldan-Varona P., Leandro D., Rodriguez-Cobo L., Lopez-Higuera J.M., Lopez-Amo M. (2021) Microdrilled tapers to enhance optical fiber lasers for sensing, *Sci. Rep.* **11**, 20408.

8 Shen F.C., Zhou K., Zhang L., Shu X.W. (2016) Switchable dual-wavelength erbium doped fibre laser utilizing two-channel fibre Bragg grating fabricated by femtosecond laser, *Laser Phys.* **26**, 105103.

9 Lei L., Li H., Shi J., Hu Q., Zhao X., Wu B., Wang M., Wang Z. (2021) Miniature Fabry-Perot cavity based on fiber Bragg gratings fabricated by Fs laser micromachining technique, *Nanomaterials* **11**, 2505.

10 Kondo Y., Nouchi K., Mitsuyu T., Watanabe M., Kazansky P.G., Hirao K. (1999) Fabrication of long-period fiber gratings by focused irradiation of infrared femtosecond laser pulses, *Opt. Lett.* **24**, 10, 646–648.

11 Bharathan G., Hudson D.D., Woodward R.I., Jackson S.D., Fuerbach A. (2018) In-fiber polarizer based on a 45-degree tilted fluoride fiber Bragg grating for mid-infrared fiber laser technology, *OSA Contin.* **1**, 1, 56–63.

12 Zhang Y.F., Lin C., Liao C., Yang K., Li Z., Wang Y. (2018) Femtosecond laser-inscribed fiber interface Mach-Zehnder interferometer for temperature-insensitive refractive index measurement, *Opt. Lett.* **43**, 18, 4421–4424.

13 Liu Y., Wang D.N. (2018) Fiber in-line Michelson interferometer based on inclined narrow slit crossing the fiber core, *IEEE Photon. Technol. Lett.* **30**, 3, 293–296.

14 Pallarés-Aldeiturriaga D., Rodríguez-Cobo L., Quintela A., López-Higuera J.M. (2017) Curvature sensor based on in-fiber Mach–Zehnder interferometer inscribed with femtosecond laser, *J. Light. Technol.* **35**, 21, 4624–4628.

15 Lin C., Liao C., Zhang Y., Xu L., Wang Y., Fu C., Yang K., Wang J., Hea J., Wang Y. (2018) Optofluidic gutter oil discrimination based on hybrid-waveguide coupler in fiber, *Lab Chip* **18**, 4, 595–600.

16 Huang B., Shu X.W. (2018) Highly sensitive torsion sensor with femtosecond laser-induced low birefringence single-mode fiber based Sagnac interferometer, *Opt. Express* **26**, 4, 4563–4571.

17 Budinski V., Donlagic D. (2017) Fiber-optic sensors for measurements of torsion, twist and rotation: A review, *Sensors* **17**, 443.

18 Smith A.M. (1980) Birefringence induced by bends and twists in single-mode optical fiber, *Appl. Opt.* **19**, 2606–2611.

19 Ulrich R., Simon A. (1979) Polarization optics of twisted single-mode fibers, *Appl. Opt.* **18**, 2241–2251.

20 Ross J.N. (1984) The rotation of the polarization in low birefringence monomode optical fibres due to geometric effects, *Opt. Quant. Electron.* **16**, 455–461.

21 Napiorkowski M., Urbanczyk W. (2021) Rigorous modeling of twisted anisotropic optical fibers with transformation optics formalism, *Opt. Express* **29**, 15199–15216.

22 Bernas M., Zolnacz K., Napiorkowski M., Statkiewicz-Barabach G., Urbanczyk W. (2021) Conversion of LP11 modes to vortex modes in a gradually twisted highly birefringent optical fiber, *Opt. Lett.* **46**, 4446–4449.

23 Yiping W., Wang M., Huang X. (2013) In fiber Bragg grating twist sensor based on analysis of polarization dependent loss, *Opt. Express* **21**, 11913–11920.

24 Roldán-Varona P., Lomer M., Algorri J.F., Rodríguez-Cobo L., López-Higuera J.M. (2022) Enhanced refractometer for aqueous solutions based on perfluorinated polymer optical fibres, *Opt. Express* **30**, 1397–1409.

25 Perez-Herrera R.A., Roldan-Varona P., Rodriguez Cobo L., Lopez-Higuera J.M., Lopez-Amo M. (2021) Single longitudinal mode lasers by using artificially controlled backscattering erbium doped fibers, *IEEE Access* **9**, 27428–27433.

26 Perez-Herrera R.A., Stancalie A., Cabezudo P., Sporea D., Neguţ D., Lopez-Amo M. (2020) Gamma radiation-induced effects over an optical fiber laser: Towards new sensing applications, *Sensors* **20**, 3017.

27 Perez-Herrera R.A., Pallarés-Aldeiturriaga D., Júdez A., Rodriguez Cobo L., Lopez-Amo M., Lopez-Higuera J.M. (2019) Optical fiber lasers assisted by microdrilled optical fiber tapers, *Opt. Lett.* **44**, 2669–2672.

28 Perez-Herrera R.A., Fernandez-Vallejo M., Diaz S., Angeles Quintela M., Lopez-Amo M., López-Higuera J.M. (2010) Stability comparison of two quadruple-wavelength switchable erbium-doped fiber lasers, *Opt. Fiber Technol.* **16**, 4, 205–211.

29 Perez-Herrera R.A., Roldan-Varona P., Galarza M., Sañudo-Lasagabaster S., Rodriguez-Cobo L., Lopez-Higuera J.M., Lopez-Amo M. (2021) Hybrid Raman-erbium random fiber laser with a half open cavity assisted by artificially controlled backscattering fiber reflectors, *Sci. Rep.* **11**, 9169.